

High-resolution imaging using lucky frame selection

This paper reports on progress towards the development of an imaging methodology which has potential for producing high-resolution imagery that has not been degraded by atmospheric turbulence. The technique relies on a well known concept called 'lucky frame selection', although uses a radically different approach. Rather than using an image based metric to determine image quality we have proposed the use of a 'phase-diversity' metric (PDM). We have shown that there are several advantages to the use of such a metric: computational speed and efficiency, insensitivity to noise, image content and distortion. These advantages have been demonstrated using real imagery. A frame composition algorithm has also been developed which builds up, over an imaging sequence, an undistorted good quality image. The technique has been demonstrated over a 4.3km ground-to-ground path with up to a factor of 2 improvement in image quality.

By

S C Woods, J G Burnett, P J Kent and A J Turner

QinetiQ Ltd., St Andrews Road, Great Malvern WR14 3PS

Introduction

Conventional imagery is degraded by atmospheric blurring limiting the range for recognition and identification. Frame selection is a concept that relies on the fact that very occasionally atmospheric turbulence ‘behaves’, so that there is a finite probability that a short exposure snapshot will not suffer from significant resolution degradation. Capturing imagery with sufficiently short exposures is the prerequisite of all so called ‘speckle imaging’ or ‘lucky imaging’ techniques. An imaging system that is able to exploit this phenomenon (i.e. is able to efficiently discriminate ‘lucky’ frames or sub-frames) would enable a significantly enhanced capability for high-resolution imaging.

The purpose of this paper is to report on the progress made since we proposed a lucky frame selection technique at last years EMRS-DTC conference [1]. In that paper the concept of a phase-diversity metric (PDM) is described and a robust practical implementation based on an ‘Image Multi-Plex’ (IMP) grating was proposed.

The concept of recovering diffraction-limited resolution from turbulence degraded imagery using a ‘speckle imaging’ approach is not new. Previous work by others in this area has concentrated on assessing and/or post-processing image, or multiple image data sets, in an attempt to determine sub-image quality or reconstruct high-resolution information. However, progress in this field has been slow and is known to suffer from some fundamental issues as well as being dependent on sophisticated (and hence slow) algorithms.

This DTC programme aims to develop an efficient and robust system based on the principles of lucky imaging although using a radically different approach. Rather than applying sophisticated algorithms to the entire image or processing large data sets of images, we have proposed the use of a ‘phase-diversity’ metric (PDM). Initially it was hoped that such a metric would be faster and more efficient than conventional image sharpness metrics and indeed we have shown that due to the simplicity of the PDM it is likely to be an order of magnitude faster. The technique may also improve efficiency since only good quality regions of the image need be readout. In this paper we report on further advantages of the PDM approach:

- The PDM has a noise response which is completely appropriate to lucky sub-frame selection
- The PDM is not sensitive to variations in image content, a known problem for image based metrics, and
- The PDM is not sensitive to atmospherically induced distortion, also a problem for image based metrics.

In addition to further theoretical analysis we also report on the development of an imager that simultaneously captures the required ‘phase-diversity’ data as well as a high-resolution ‘in-focus’ image, albeit degraded by atmospheric turbulence. The imager is based on the use of an IMP grating, which provides a simple and robust optical design. Although this particular design has a limited spectral bandpass of operation for passively illuminated objects, the system has been demonstrated and data sets have been captured and used to assess PDM performance and to initiate development of an image composition algorithm; taking the best bits from each frame and building up a good quality image.

This imager has been used to capture imagery over a close to ground 460m and 1.2km path at QinetiQ Pershore. The Pershore data sets have been used to develop the current data processing methodology. The imager has also been used to capture imagery at the Dstl Porton Down ground-to-ground ranges covering 1.4km and 4.3km during the ‘Hydra Vision’ trials in March 2008 [2]. The later data sets have successfully demonstrated the technology (PDM and image composition algorithms) over operationally useful ranges. This paper will report on the results for the 4.3km range.

The PDM imager

The imaging system comprises an Orion Optics Maksutov-Cassegrain telescope with an aperture of 140mm and an $f/14$ focal plane. Relay optics provides an image on a CCD camera [3] at $f/20$ magnification. The Rayleigh Diffraction Limit (RDL) is $4.64\mu\text{rad}$ and the image is Nyquist sampled by the camera (pixel FOV = $2.26\mu\text{rad}$). An IMP grating in the re-imaged pupil plane provides the angular separation and defocusing of the phase-diversity images. Binary phase IMP gratings were used to provide different levels of defocus for the phase-diversity images. Much of the imagery was captured using 0.8 and 1.2 waves (PV) of defocus. The grating phase step was chosen to ensure $\sim 33\%$ transmission efficiency into the zero and ± 1 diffracted orders. The angular separation (or FOV) of the images on the CCD camera was 200 pixels. A field stop in the first image plane restricts the FOV to prevent overlap between the in-focus zero-order and the defocused ± 1 order phase-diversity

images. A high-transmission ($T > 95\%$) filter centred on 532nm restricts the bandpass to 25nm to reduce the effect of chromatic dispersion in the phase-diversity images. The completed system is shown below:

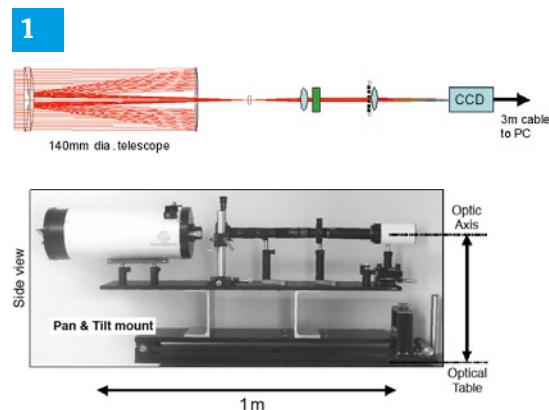


Illustration & side view of the imaging system. The breadboard is attached to a pan and tilt mount for accurate pointing.

The image data from the camera is streamed to disk at a frame rate of 10fps (no pixel binning) via a custom Labview interface. Typically ~ 1000 frames are captured per data set which is then processed off-line.

PDM versus Image Sharpness Metrics

The initial analysis of the data was intended to demonstrate the correlation between the phase-diversity metric (PDM) and the well-known I^2 image sharpness metric (ISM). This was based on the assumption that the ISM would provide a reliable measure of image quality against which the PDM could be compared to determine its effectiveness in selecting regions of high image quality.

The first stage of the data analysis was to extract the zero-order and phase-diversity images from each frame at a size of 200×200 pixels. The images were then subdivided into sub-images of typically 8×8 pixels, and both the ISM and the PDM calculated for each sub-image. The ISM is calculated from the zero-order sub-images, and is given by

$$ISM = \frac{\sum_{pixels} I^2}{\left(\sum_{pixels} I\right)^2}$$

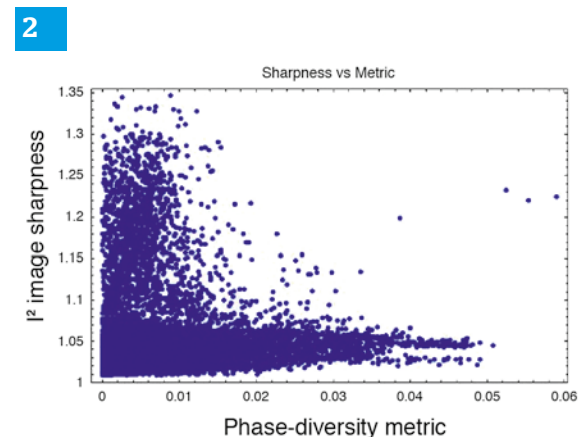
The denominator of the above expression is there to normalize the ISM, without which the ISM would scale proportionally to the square of the image brightness. The ISM increases with increasing image sharpness.

The PDM is calculated from the phase-diverse images, and is given by

$$PDM = \frac{\sum_{pixels} |I_1 - I_2|}{\sum_{pixels} (I_1 + I_2)}$$

where the subscripts 1 and 2 refer to the two phase-diversity images. Note that the PDM is also normalized. The PDM decreases with increasing image quality.

The ISM and PDM were calculated for all sub-images in every frame of the data set, and the resulting values plotted as ISM vs PDM. A typical example of such a plot is shown in Figure 2.



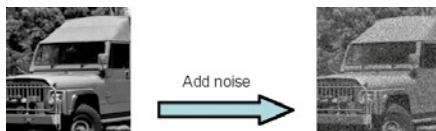
I^2 sharpness metric vs phase-diversity metric.

The results show a very poor correlation between ISM and PDM. Subsequent inspection of the raw data revealed that some visually poor images were achieving some of the highest ISM values. Further investigation suggested that the assumption that the ISM would provide a reliable measure of image quality is fundamentally flawed under conditions of varying image brightness. The reasons for this are discussed in the next section.

Noise response of image quality metrics

Image quality metrics based on direct analysis of the image are susceptible to noise in the image, as this can change the apparent “amount of detail” in the image irrespective of wavefront distortion. The I^2 sharpness metric sees noise as an increase in detail, as indicated in Figure 3.

3



Visually, the noiseless image on the left is of higher quality. However, the ISM is higher for the image on the right, due to the added “detail” of the random noise.

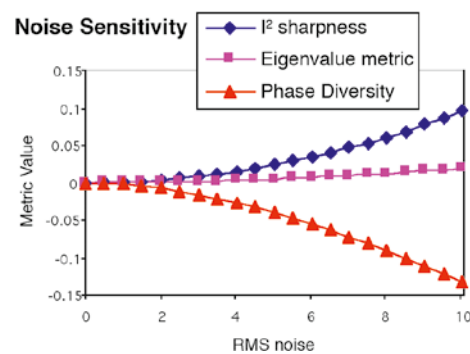
Although we do not expect significant fluctuations in image noise from frame to frame, there will be variations in image intensity due to changing illumination levels. The normalization of the ISM means that the noise level in low intensity images is effectively amplified relative to that in high intensity images. Thus, an image with low intensity (i.e. low SNR) has a higher ISM value than the same image with high intensity (high SNR). This suggests that the ISM is a poor choice of metric for sub-frame selection, since it will preferentially select sub-frames with low SNR. This also means that the ISM is a poor choice of metric against which to evaluate the phase-diversity approach to sub-frame selection.

An alternative image quality metric, which is expected to be nearly noise-invariant, is the eigenvalue sharpness metric (ESM) [4]. The ESM is calculated by forming the covariance matrix of the image rows (or columns) and calculating its eigenvalues. The ESM is the sum of the first “few” highest eigenvalues. This approach is essentially performing a Principal Components Analysis of the image rows, with the ESM measuring how much of the variance between rows is contained within the first few principal components.

The ESM is probably not a practical metric for real-time sub-frame selection, since the formation of the covariance matrix and calculation of its eigenvalues is a relatively slow process compared to computation of simpler metrics such as the ISM. However, the robustness of the ESM to varying SNR makes it a better baseline metric than the ISM for the purpose of evaluating the phase-diversity technique.

The PDM is not invariant to noise. However, since the noise is uncorrelated between the two phase-diverse images, adding noise (decreasing SNR) will tend to make the two images more different, increasing the PDM. The PDM decreases with increasing image quality, so the PDM sees decreasing SNR as decreasing image quality. This is the trend one would prefer for a frame selection process. Patches dominated by low SNR are considered ‘unlucky’ and would not be used to update the composite frame. The noise response of the ISM, ESM and PDM are shown in Figure 4.

4



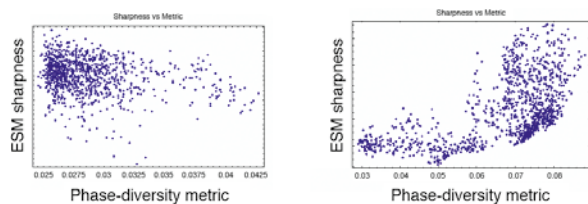
Effect of noise on image quality as measured by ISM, ESM and PDM. The ISM considers image quality to increase with increasing noise. The ESM is almost invariant to noise. The PDM regards image quality as decreasing with increasing noise.

For the graph in Figure 4 the metrics have all been offset and scaled to give the same results for a given sharp and blurred image. Thus, the value on the y-axis is a measure of image quality, rather than the raw metric values.

Correlation between PDM and ESM

For the reasons outlined above we believe that the ESM will be a better baseline metric than the ISM, at least in terms of invariance to noise. The initial data analysis was repeated, except the ESM was used in place of the ISM. This analysis revealed a much clearer correlation between the PDM and the baseline ESM in some data sets, however in other data sets the correlation was very poor. Some typical results corresponding to both these cases are shown in Figure 5.

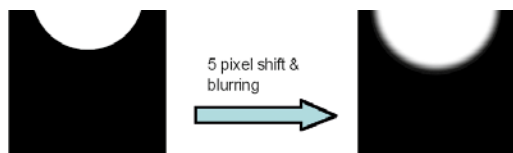
5



ESM vs PDM in two data sets. In the data on the left, a good correlation is seen, with the highest values of ESM corresponding to the lowest values of the PDM. In the data on the right the correlation is very poor.

The impact of varying image content on the image quality metrics was investigated with a simple test image comprising a black background with a white circular object at the edge of the FOV. A second test image was constructed by shifting the circular object up by 5 pixels and applying a Gaussian blur. This is shown in Figure 6. The ESM was calculated for both test images, and the blurred image was found to give the higher ESM value, indicating a better image. The same result was obtained with the ISM. The reason for this is that the change in image content caused by shifting the circular object by 5 pixels has a greater effect on the ESM and ISM than the reduction in image sharpness caused by the blurring.

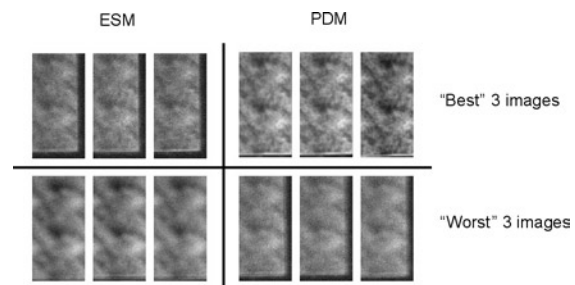
6



The ESM and ISM both incorrectly rate the image on the right as sharper than the image on the left.

A confirmation of this effect in a real data set can be seen in Figure 7. A data set was analysed by calculating the ESM and PDM across the whole FOV for each frame in the set. The best and worst three images according to both metrics were then noted. The results show that while the PDM does a good job of selecting the best and worst frames, the ESM has been confused by the changing image content as the edge of the target board appears in the FOV. Indeed, the “best” images according to the ESM are among the least sharp in the entire data set.

7

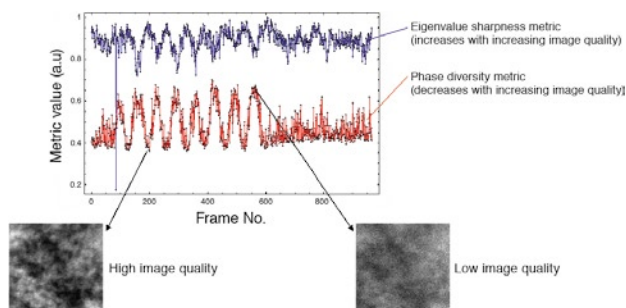


Best and worst images from a data set according to the ESM and the PDM. The ESM is ‘fooled’ by changing image content whilst the PDM is not.

Image quality metrics based on direct analysis of the image are thus susceptible to variations in image content, as this can change the “amount of detail” in the image irrespective of wavefront distortion. Due to atmospheric distortion (anisoplanatic jitter), the features present in a particular sub-frame region will differ from frame to frame. Image quality metrics based on direct analysis of the image are dominated by this effect, and will select sub-frames according to the features therein, rather than the quality with which those features are imaged. The phase diversity approach does not have this problem, since it analyses the symmetry of the PSF either side of focus, rather than the image content itself. (i.e. phase diversity looks for sub-frames imaged with a near-flat wavefront, regardless of what is being imaged).

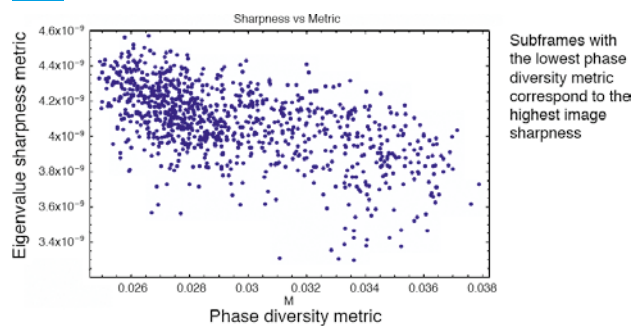
A confirmation of the correlation between the ESM and PDM in the absence of this effect was obtained from a specially captured data set. In this data set the camera was carefully aligned to the centre of the target board to prevent sharp edge features appearing in the FOV. Also, the camera was manually adjusted through focus several times during capture of the first 600 frames. This provides data in which the dominant aberration is the slowly varying isoplanatic focus error. The results of the analysis are shown in Figures 8 and 9, and clearly demonstrate a good correlation between the PDM and the ESM.

8



Comparison of PDM (red) and ESM (blue) as a function of time (frame No.) The camera was manually cycled through focus during capture of the first 600 frames.

9



Correlation between the PDM and ESM in a data set with isoplanatic aberrations and no substantial variations in image content (i.e. edges moving in and out of the FOV). The graph shows the desired result – the highest quality images (high ESM) are those with the lowest values of the PDM.

The analyses above give a high degree of confidence that the PDM provides a reliable method for selecting lucky sub-frames. Importantly, they also reveal some significant advantages of the PDM over other image quality metrics in terms of its response to varying SNR and image content. However, the limitations of the other image quality metrics mean that a direct sub-frame by sub-frame comparison cannot be used to obtain a qualitative assessment of the performance of the phase-diversity technique, since neither the ISM or ESM provide a reliable baseline metric.

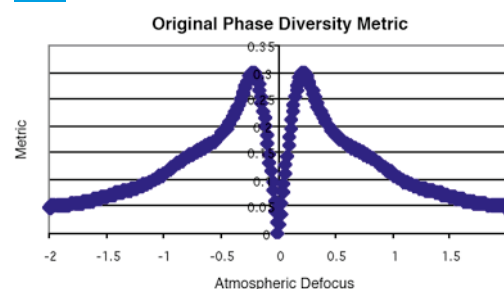
Due to the difficulty in obtaining a reliable baseline metric to compare phase diversity against in the presence of atmospheric distortion, it was decided that the most appropriate test of the phase diversity approach would be to proceed with the sub-image registration and image composition tasks to generate full-frame lucky images, which can then be compared with those generated via the ISM and/or ESM techniques.

Combined PDM

Analysis of initial composite frames assembled from the trials data revealed that the phase-diversity metric was occasionally selecting sub-frames of very poor image quality. The reason for this can be understood by considering the behaviour of the phase-diversity metric when the image degradation is very high. Essentially, if the atmospherically induced aberrations are substantially stronger than the defocus introduced by the IMP grating, the appearance of the phase-diversity images is dominated by the atmospheric aberration and the two images appear very similar. This means that the phase-diversity metric is low, a condition which is interpreted as high image quality in the sub-frame selection algorithm.

The response of the phase-diversity metric to increasing atmospheric aberration is shown in Figure 10.

10



Phase-diversity metric as a function of atmospheric defocus.

It is clear that the metric has the desired properties for low levels of atmospheric aberration, with the metric value increasing with increasing image degradation. However, for large amounts of atmospheric aberration the metric starts to decrease as the phase-diversity images start to look similar again.

In order to resolve this issue, a secondary selection stage has been considered, which includes the zero-order in the comparison of the images. In the low aberration case, the zero-order looks significantly different from the phase-diversity images (since it is in focus whereas the phase-diversity images are out of focus). However, in the strong aberration case, the zero-order appears very similar to the phase-diversity images (since they are all highly blurred). Thus, a comparison of the zero-order image to the phase-diversity images can discriminate between the low and strong aberration cases. To summarise:

Aberration	PD images	Zero-order image
Low	Similar	Different
Medium	Different	Different
High	Similar	Similar

In a practical real-time system, the comparison of the zero order image would be implemented as a secondary sub-frame selection process on the reduced data set selected by the PDM. Since the number of sub-frames in this reduced data is a fraction of the raw data, this second stage of selection will not significantly increase the computation time. However, for ease of data processing with our existing software, we have implemented a “combined phase-diversity metric” (CPDM) which effectively combines both selection stages into one.

The original metric takes the form:

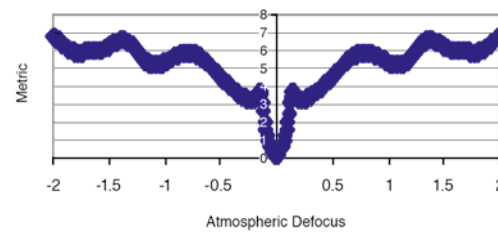
$$metric = \sum_i |P_i - M_i|$$

where P_i and M_i are the i 'th pixel values in the normalised +1 and -1 orders. The combined metric takes the form:

$$metric = \frac{\sum_i |(P_i - M_i)|}{\sum_i |(Z_i - \frac{1}{2}(P_i + M_i))|}$$

where Z_i is the i 'th pixel value in the zero-order. The numerator is the original metric, but the CPDM includes the denominator term which decreases as the zero-order becomes similar to the phase-diversity images. The response of the CPDM to increasing atmospheric aberration is shown in Figure 11.

11

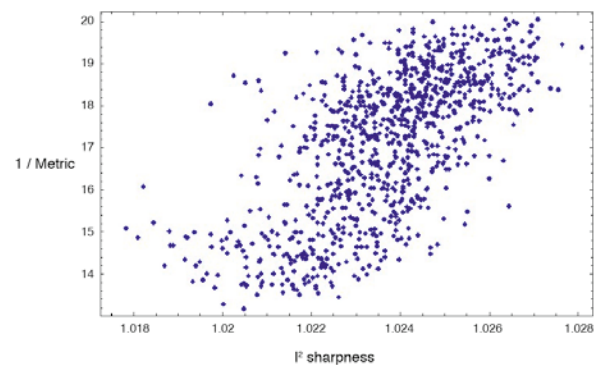


CPDM as a function of atmospheric defocus.

It is clear that the CPDM provides a much better response for large atmospheric aberrations than the original PDM. Rather than reaching a maximum and then decreasing, the CPDM continues to increase (with slight oscillations) with increasing aberration.

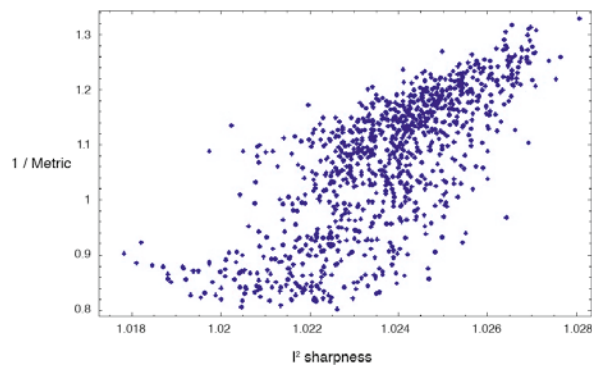
The CPDM was compared against the original metric by analysing a trials data set using both metrics, and the ISM. The results are shown in Figures 12 and 13. Note that in these Figures the inverse of the metric has been plotted, which increases with increasing image quality.

12



PDM vs ISM.

13



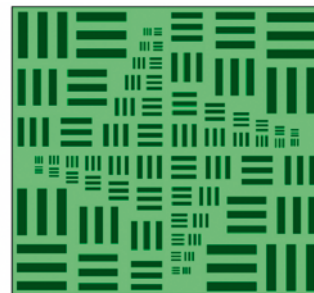
CPDM vs ISM.

It is clear that in both cases, the highest sharpness values correspond to the highest inverse metric values. However, with the original metric, the highest inverse metric values correspond to a wide range of sharpness values. Thus, sub-frame selection based on this metric will pick out some regions of poor image quality along with the regions of good image quality. By contrast, with the CPDM the highest inverse metric values correspond only to the sharpest images. Thus, sub-frame selection based on the CPDM will pick out only regions of good image quality, as required.

Porton Down trials

As mentioned in the Introduction the imaging system was also used to capture data during the 'Hydra Vision' trials at Dstl Porton Down in March 2008. All the software processing algorithms that had been developed using data from Pershore (up to 1.2km) could now be tested with data collected over a 4.3km range. The geography of the 4.3km path is mainly over grassland and crosses a shallow valley. The weather conditions during the trials were generally overcast, although some data was collected during sunny intervals. The object chosen for observation was a resolution chart target board based on standard triplet bar groups (see Figure 14). Just above this target board was also placed a 30mm square fluorescent card on black background to provide a passive point source for estimating turbulence strength.

14



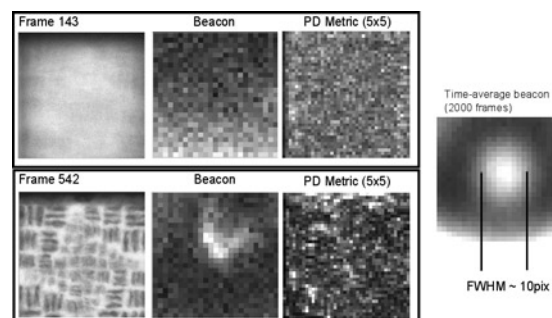
2m x 2m
Bar target groups (USAF):
(-5; 5,3,1)(-6; 5,3,1)(-7; 5,3,1)
Bar period: 20.16mm to 128mm
(RDL to x 6.35 RDL)

Resolution target board used for imaging over a 4.3km range.

This paper will report on the results from imagery captured over the 4.3km path and in particular two data sets which will be referred to as A and B. Set A was recorded at 14:23 17th March, and represents the 'worst' conditions (recorded during sunny intervals) and the frame exposure time was 5.6ms. Set B was recorded at 13:08 on 18th March when the turbulence strength was less (overcast) and the frame exposure was 30ms. The exposure times chosen were the shortest possible without significantly impacting on the SNR of the images.

An example of 'bad' and 'good' frames, from set A, is shown in Figure 15. Included in this Figure are also the corresponding beacon images, CPDM bitmap values (based on 5x5 regions) and the time averaged beacon image which is used to estimate turbulence strength. Turbulence strength levels can also be subjectively estimated from the resolution target board imagery.

15



Sample 'bad' and 'good' frames from data set A.

Estimating C_n^2 values from beacon measurements can be achieved as follows. An expression relating the FWHM of the long-exposure point-spread-function β (in radians) to the Fried parameter r_0 is given by [5]

$$\beta = 0.98 \frac{\lambda}{r_0}$$

Here λ is the wavelength and for these trials is taken as 532nm (centre wavelength of narrowband 25nm filter used). The Fried parameter can be related to a path-averaged C_n^2 value, where L is the path length, via the spherical-wave structure function and therefore a value for C_n^2 can be estimated from the following equation [6, 7]

$$C_n^2 = 0.165 \frac{\lambda^{\frac{1}{3}} \beta^{\frac{5}{3}}}{L}$$

For data set A the FWHM of the long exposure PSF is ~ 10 pixels. This translates into a Fried parameter of ~ 23 mm ($D/r_0 \sim 6$; this is consistent with assessment of resolution based on resolution targets described below) and a C_n^2 of $\sim 5.6 \times 10^{-15} \text{ m}^{-2/3}$ for the 4.3km range. This is representative of weak turbulence which is also consistent with the environment and conditions at the time of the trial. This is also consistent with the relatively low number of frames needed to build up a composite frame as predicted by Fried's probability equation [8] for the degree of turbulence at $D/r_0 \sim 6$, i.e. ~ 50 frames are required to assemble a lucky image.

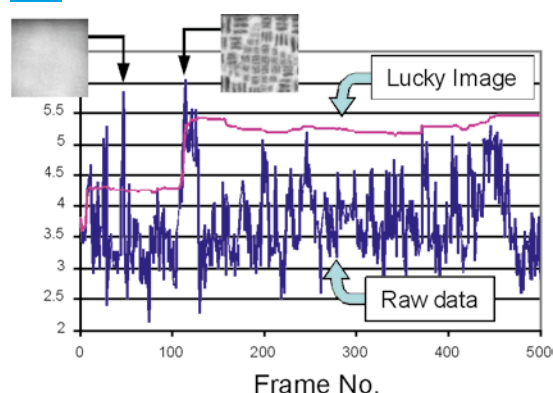
Lucky image composition

The current processing applied to the phase diverse imagery consists of the following steps:

- The source imagery is split into the zero-order and phase diversity images;
- Phase diversity metric 'images' are computed from the imagery;
- All zero-order images are summed (integrated over time) to produce a low resolution (due to atmospheric blurring) but generally geometrically correct reference image;
- Each zero-order image is sequentially registered against the reference image. This alignment process is based on optical flow (intensity difference minimisation) methods using a geometric distortion model encompassing local translation. Some correction for gross brightness changes is also applied;
- The phase diversity metric images are also warped into alignment with the reference image using the alignment information computed from the zero-order images;
- The final lucky image is assembled by scanning through the aligned image data sets, extracting sections of the imagery where the phase diversity metric is optimal.

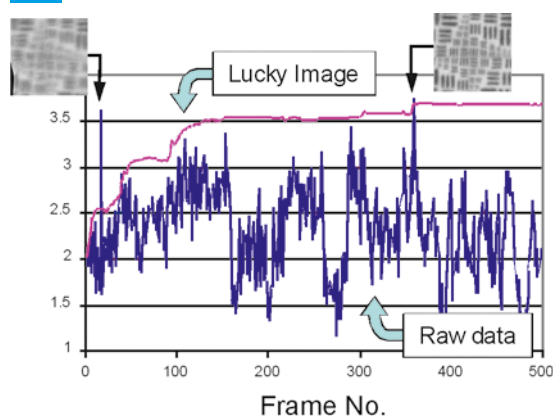
A plot of the progression of this process with time (frame No.) is a useful demonstration of the technique and its robustness. This is illustrated for both data sets A and B in Figures 16 and 17 respectively where the ESM has been used to compare the sharpness of the raw data and the progression of the composite lucky image. In both cases it is clear that the image quality of the composite lucky image converges to a maximum. In particular it is clear that when periods of good images appear then the lucky image improves correspondingly. However, during periods of bad imagery the lucky image is unaffected. It is interesting to note that the ESM does not necessarily correlate with good image quality. Occasionally some frames appear that are clearly 'bad' although the ESM suggests they contain good quality data. The PDM ignores these glitches.

16



Progression of image sharpness (as determined using ESM) for raw data and the composite lucky frame for data set A. Two frames have been picked out that illustrate poor ESM discrimination compared to the PDM.

17



As Figure 16, except for data set B.

Both sets of data converge to a 'best' lucky frame after ~ 120 frames, although this is very much dependent on the arbitrary starting point chosen. The period between 'step improvements' (particularly in Figure 17) is ~ 50 frames, which, as suggested in the previous Section, is consistent with what the Fried equation predicts.

Quantitative resolution comparison

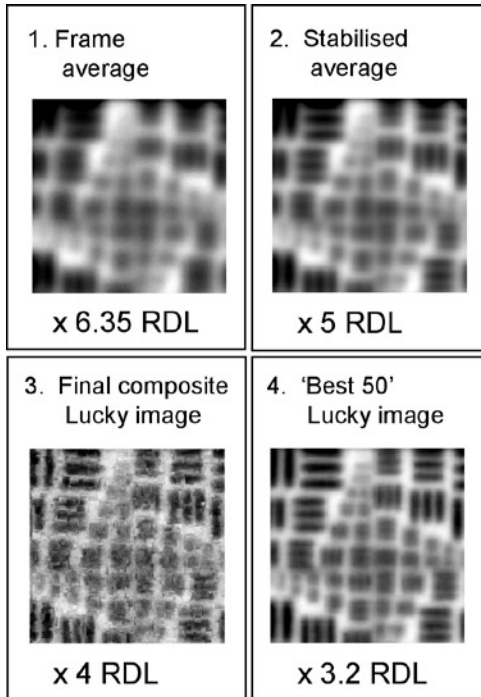
To attempt to quantify the resolution gains provided by phase-diversity lucky imaging, the following images were assembled and analysed for the two data sets:

1. The average of all raw frames (this corresponds to the long-exposure image).
2. The average of all frames after stabilisation and distortion correction (this corresponds to the best image attainable from snapshot imaging without frame selection).
3. The 'final composite' lucky image, consisting of the single best sub-frames from the data set in each sub-region.
4. The 'best 50' lucky image, consisting of the mean of the 50 best sub-frames from the data set in each sub-region (this provides a composite lucky image with improved SNR but potentially at the cost of a slight decrease in resolution)

Each of these images was visually inspected to identify the smallest set of bars which can be resolved. The results are shown in Figures 18 and 19.

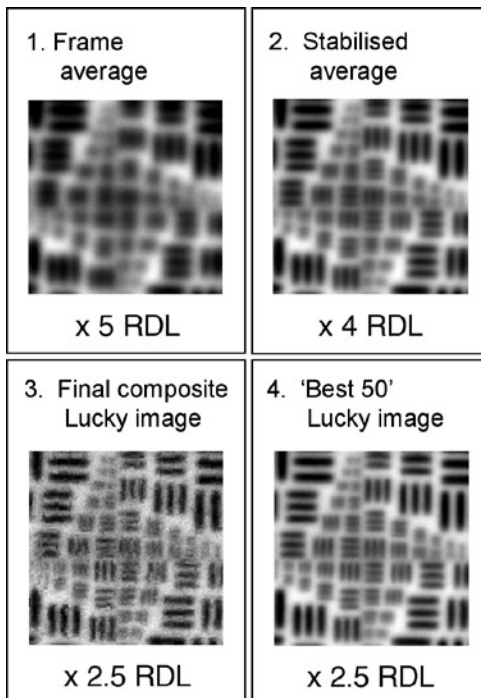
Figures 18 and 19 clearly show an improvement in image quality which is at least a factor of 2 better than what would be achieved without lucky imaging. It is noted however that we are still not achieving a diffraction limited image and the most likely explanation is that the exposure time is still too long to sufficiently 'freeze' the effects of turbulence. The exposure time in the current system is limited by low SNR which is mainly due to the use of a relatively narrow spectral filter.

18



Frame averages and composite images for set A. The RDL at 4.3km is 20mm.

19



Frame averages and composite images for set B.

Conclusions

The phase-diversity approach to lucky sub-frame selection has been shown to have several advantages over standard image-based metrics:

- The PDM has a noise response which is completely appropriate to lucky sub-frame selection
- The PDM is not sensitive to variations in image content, a known problem for image based metrics, and
- The PDM is not sensitive to atmospherically induced distortion, also a problem for image based metrics.

A combined phase-diversity metric has been identified which permits the technique to work even when very blurred frames are present in the data set.

An imager was built to capture the necessary data to develop and demonstrate the technique. Results from the Hydra Vision trials over a 4.3 km path at Porton Down have proved the robustness of the technique and provided final imagery which is a factor of 2 better in resolution than what would be achieved without lucky imaging.

Acknowledgements

The work reported in this paper was funded by the Electro-Magnetic Remote Sensing (EMRS) Defence Technology Centre, established by the UK Ministry of Defence and run by a consortium of SELEX Galileo, Thales UK, Roke Manor Research and Filtronic.

We also acknowledge the efficiency and support of all the Dstl staff during the 'Hydra Vision' trials at the Dstl facilities at Porton Down [2].

References

1. S. C. Woods, J. G. Burnett, A. M. Scott, 'Efficient technique for lucky frame selection using phase diversity images', Proceedings of the 4th EMRS DTC Technical Conference 2007.
2. R. C. Hollins, 'Technologies Trial Results', 5th EMRS DTC Technical Conference 2008.
3. QImaging Retiga EXi 12-bit monochrome CCD camera. Sony ICX285AL chip: 1393 x 1040, 6.45 μ m pixels, 60% QE at 532nm.
4. Wee et al., Information Sciences, **177** (2007) 2533–2552.
5. P. Dierickx, 'Optical performance of large ground based telescopes', J. Mod. Opt., **39**, no. 3, pp569-588 (1992).
6. J.W. Goodman, 'Statistical Optics', Chapt. 8 (Wiley, New York, 1985).
7. M.C. Roggemann and B. Welsh, 'Imaging Through Turbulence', Chapter 3 (CRC press, New York, 1996).
8. Fried, D. L. 'Probability of getting a lucky short-exposure image through turbulence'. J. Opt. Soc. Am. 1978, 68, 1651–1658.